Hindawi
International Transactions on Electrical Energy Systems
Volume 2022, Article ID 4176869, 12 pages
https://doi.org/10.1155/2022/4176869

Research Article

A New Locating Method of Break Faults in an Active Distribution Network Based on Distributed Generator Monitoring

Yang Xiao, Jinxin Ouyang, and Xiaofu Xiong

State Key Laboratory of Power Transmission Equipment & System Security and New Technology, School of Electrical Engineering, Chongqing University, Chongqing 400044, China

Correspondence should be addressed to Jinxin Ouyang; jinxinoy@163.com

Received 18 October 2021; Accepted 28 November 2021; Published 31 January 2022

Academic Editor: Akshay Kumar Saha

Traditional distribution networks are transforming into active distribution networks (ADNs) with the advancement of distributed generators (DGs). Break faults that lead to voltage and current imbalances and fluctuations threat the safety of sensitive power electronic equipment in ADNs. However, locating break faults in ADNs remains a challenge under the influence of DG fault polymorphism. This paper proposes a new method to locate break faults by monitoring information of DG current based on the observability of ADNs. The DG equivalent model is established based on the DG output characteristics under the presence of a single-phase break fault. The characteristics of the fault current contributed by DG are analyzed. An identification method of break faults is proposed based on the variations in DG current. Thus, a fault-locating matrix algorithm is proposed combined with current information and location information of DGs. The simulation results demonstrate that the proposed method can locate break faults quickly and accurately. The method is not affected by topology and changes of DG output and load.

1. Introduction

The scale of distributed generator (DG) access to the distribution network is expanding along with the development and increasing application of renewable energies. Apart from solving energy shortage and environmental pollution problems, DGs have a significant role in protecting and controlling distribution networks [1, 2]. DGs have significantly changed the fault characteristics of distribution networks, thereby introducing challenges in fault identification and location. Traditional distribution networks have been transformed into active distribution networks (ADNs) with a high proportion of DGs. ADNs can actively manage DGs, controllable loads, and switches and flexibly adjust the network topology, thereby providing a new means for protection and control.

The existing fault location methods for distribution networks mainly include the impedance method [3], traveling wave method [4], active injection method [5], matrix algorithm [6], and artificial intelligence algorithm [7]. Many scholars have recently examined these methods while considering the influence of DGs. The study in [8] proposed a method that compensates for fault impedance and errors associated with DGs for distance relays yet requires a multipoint simultaneous measurement. The work in [9] proposed a fault location method based on voltage sag measurements that reduces voltage measurement requirements and is proven suitable for various types of DGs. The study in [10] proposed a heuristic algorithm based on bus currents and voltages that employs a pattern search method to estimate the optimal fault point. However, the reliability of such algorithm is affected by the inaccuracy of feeder parameters and the DG equivalent model. On the basis of the block-sparse Bayesian learning method, the study in [11] formulated the fault location problem as the estimation of a block-sparse fault injection current signal that does not require a DG equivalent yet relies on μPMUs. However, most of the existing fault location methods are aimed at short-circuit faults, and only few of these methods consider break faults. Given that the equivalent circuit and electrical characteristics of short-circuit and break faults completely differ, short-circuit fault location methods cannot be used to identify and isolate break faults.

Distribution lines are susceptible to lightning strikes, external forces, electrical effects, etc., resulting in break faults. With the increasingly complex topology of distribution networks, break faults have been frequently reported in recent years. Break faults lead to a phase-deficient operation and generate negative sequence components that affect power quality and threaten personal safety. ADNs contain many sensitive power electronic equipment, which can be easily damaged by severe voltage and current fluctuations caused by break faults [12]. At present, break faults are mainly identified by detecting abnormal voltages in substations and checked by manual line patrolling [13]. However, this method cannot be easily adapted to the modern distribution networks given its time consumption, poor economy, and low reliability.

Only few studies have examined break faults in distribution networks. For instance, the authors of [14, 15] analyzed the voltage and current characteristics of break faults in a small current grounding system. The study in [16] easily realized break fault line selection given that the negative sequence current of a fault line is much larger than that of a nonfault line. Meanwhile, the work in [17] used the decrease in fault phase current and the phase difference of nonfault phase currents to realize break fault line selection. The study in [18] proposed a break fault location method based on the correlation coefficient of the negative sequence voltage and current. The study in [19] used the zero sequence voltage-amplitude difference between the power and load sides to locate the break fault section. The study in [20] realized break fault detection and location by using intelligent algorithms. However, DGs are very sensitive to the terminal voltage. The voltage drops and imbalances caused by break faults can lead to variations in DG output, which inevitably change the fault characteristics of the distribution network. However, the influence of DGs is not considered in existing break fault location methods, and only few studies have examined the DG output characteristics and equivalent modeling methods.

Given their weak characteristics, accurately locating ADN break faults under the randomness and polymorphism of DGs presents a challenge. With the excellent controllability of ADNs [21], this paper proposes a break fault location method for ADNs based on DG monitoring. Unlike traditional methods that take DG fault output as disturbance in fault identification, this paper uses rich DG fault output information to quickly and accurately locate break faults. The rest of the paper is organized as follows: Section 2 analyzes the DG current characteristics of the break fault in a distribution network and establishes an equivalent model. On the basis of the ADN break fault compound sequence network, Section 3 deduces the analytical expressions of the DG current when a break fault occurs upstream and downstream of the DG. Section 4 constructs a fault identification criterion based on the characteristics of the variation in DG fault current. In Section 5, a new break fault location matrix algorithm for ADNs is proposed. Section 6 presents the simulation results of the proposed method. Conclusions are drawn in Section 7.

The main contributions of this paper are as follows: the equivalent model of DG under the break faults in the distribution network is established. The break fault characteristics of ADNs with consideration of the impact of DGs are obtained. A new method for break fault identification based on DG current is proposed. The method is not affected by the changes of ADN topology, load, and output of DG and has high reliability. A new matrix algorithm for break fault location according to DG current is proposed. The fault location can be realized by simple matrix calculation without mathematical complexity and does not rely on external devices and is highly feasible.

2. Equivalent DG Model under the Presence of Break Faults

DGs can be divided into the asynchronous motor interface and the inverter interface based on the ways of grid connection. The asynchronous motor interface DGs mainly include doubly fed wind turbines, whereas the inverter interface DGs mainly include photovoltaic power, direct-drive wind turbine, microturbine, and energy storage. The stator of the doubly fed wind turbine is directly connected to the power grid, and the rotor is connected by a back-to-back converter. Given the limited exchange capacity of the grid-side converter (GSC), the GSC current is much lower than the stator current. Therefore, the GSC current can be ignored [22]. In a normal operation, the doubly fed wind turbine output tracks the reference values and the d- and q-axis components of the stator current can be expressed as

$$\begin{cases} i_{ds} = \dfrac{P_{\text{ref}}}{1.5u_s}, \\ \\ i_{qs} = \dfrac{Q_{\text{ref}}}{1.5u_s}, \end{cases} \tag{1}$$

where i_{ds} and i_{qs} denote the d- and q-axis components of the stator current, respectively, u_s is the terminal voltage amplitude, and P_{ref} and Q_{ref} are the reference active and reactive power values, respectively.

The three-phase voltage becomes nonsymmetrical when a break fault occurs. The positive sequence voltage drops, and negative and zero sequence voltages are generated. The drop in the positive sequence voltage is usually small under the presence of a single-phase break fault. By relying on the millisecond-level response and regulation capability of converters, DGs quickly enter the fault steady state [23]. In case of a large drop in the positive sequence voltage, DG protection or control can quickly act to avoid fault impact and then exit within a few tens of milliseconds to restore DG control performance and enter the steady state. To avoid the negative sequence current from affecting the stability, dynamic performance, and safety of power electronic equipment, DGs are generally equipped with negative sequence suppression control [24, 25]. In case the break fault is in a steady state, the negative sequence current of DGs is 0.

The rotor-side converter of the doubly fed wind turbine generally adopts a stator-flux-oriented vector control, which

means that the q-axis component of the stator flux is 0. According to the mathematical model of a doubly fed wind turbine [26], the d- and q-axis positive sequence components of the rotor current in the case of a steady-state break fault are formulated as

$$\begin{cases} i_{dr+} = \dfrac{\psi_{s+}}{L_m} - \dfrac{Q_{\text{ref}} L_s}{1.5 L_m u_{s+}}, \\ i_{qr+} = -\dfrac{P_{\text{ref}} L_s}{1.5 L_m u_{s+}}, \end{cases} \tag{2}$$

where L_s and L_m are the stator and mutual inductances, respectively, ψ_{s+} is the positive sequence component of the stator flux under a break fault, and u_{s+} is the positive sequence component of the terminal voltage under a break fault. Subscripts + and − denote the positive and negative sequence components, respectively.

Equation (2) is then substituted into the stator voltage and flux linkage equations of the doubly fed wind turbine. The d- and q-axis positive sequence components of the stator current in the break fault steady state are

$$\begin{cases} i_{ds+} = \dfrac{P_{\text{ref}}}{1.5 u_{s+}}, \\ i_{qs+} = \dfrac{Q_{\text{ref}}}{1.5 u_{s+}}. \end{cases} \tag{3}$$

The inverter interface DG is connected to the power grid by the converter. The positive and negative sequence components of the inverter output are independently decoupled. Under a negative sequence suppression control, the power equation can be expressed as [27]

$$\begin{cases} P_{\text{ref}} = 1.5\left(u_{sd+} i_{dI+} + u_{sq+} i_{qI+}\right), \\ Q_{\text{ref}} = 1.5\left(u_{sq+} i_{dI+} - u_{sd+} i_{qI+}\right), \end{cases} \tag{4}$$

where $u_{s\,d+}$ and u_{sq+} are the d- and q-axis components of terminal voltage and i_{dI+} and i_{qI+} are the d- and q-axis components of the inverter output current, respectively.

The inverter interface DG adopts vector control based on the grid voltage orientation, which means that the q-axis component of the terminal voltage is 0. The current of the inverter interface DG in the break fault steady state can be expressed as

$$\begin{cases} i_{dI+} = \dfrac{P_{\text{ref}}}{1.5 u_{s+}}, \\ i_{qI+} = -\dfrac{Q_{\text{ref}}}{1.5 u_{s+}}. \end{cases} \tag{5}$$

Equations (2)–(5) show that the DG output current is determined by the terminal voltage and the active and reactive power reference values in the break fault steady state. These active and reactive power reference values are usually adjusted according to the preset strategy. Given the fast response of converters, these reference values can be treated as constant. DG can be equivalent to a positive sequence current source controlled by the terminal voltage in the break fault.

3. Analysis of Active Distribution Network Break Faults

The fault phase current is 0, and the nonfault phase voltage is continuous at the fracture under the single-phase break fault. The boundary condition can be set as follows using the symmetrical component method:

$$\begin{cases} \dot{I}_{f1} + \dot{I}_{f2} + \dot{I}_{f0} = 0, \\ \Delta\dot{U}_{f1} = \Delta\dot{U}_{f2} = \Delta\dot{U}_{f0}, \end{cases} \tag{6}$$

where $\dot{I}_{f1}$, $\dot{I}_{f2}$, and $\dot{I}_{f0}$ denote the positive, negative, and zero sequence currents at the fault point, respectively, and $\Delta\dot{U}_{f1}$, $\Delta\dot{U}_{f2}$, and $\Delta\dot{U}_{f0}$ are the positive, negative, and zero sequence voltage differences across the fracture.

When the break fault occurs upstream of DG, by ignoring the influence of line impedance, the composite sequence network can be established as shown in Figure 1(a). $\dot{U}_N$ denotes the system voltage of ADN, $\dot{I}_S$ denotes the bus current, and $\dot{I}_{uf}$ denotes the DG current in the case of upstream break fault, which is computed as the ratio of complex power S_{DG} to terminal voltage $\dot{U}_{uf}$, where $S_{\text{DG}} = P_{\text{ref}} - jQ_{\text{ref}}$. According to Kirchhoff's law, the relationship between voltage and current is expressed as

$$\begin{cases} \dot{U}_N = \dot{I}_S Z_{S1} + \left(\dot{I}_S - \dfrac{\dot{U}_N - \dot{I}_S Z_{S1}}{Z_{iM1}}\right) \cdot (Z_2 \| Z_0) + \left(\dot{I}_S - \dfrac{\dot{U}_N - \dot{I}_S Z_{S1}}{Z_{iM1}} + \dot{I}_{uf}\right) Z_{iN1}, \\ \dot{U}_{uf} = \dot{I}_{uf} Z_{T1} + \left(\dot{I}_S - \dfrac{\dot{U}_N - \dot{I}_S Z_{S1}}{Z_{iM1}} + \dot{I}_{uf}\right) Z_{iN1}, \end{cases} \tag{7}$$

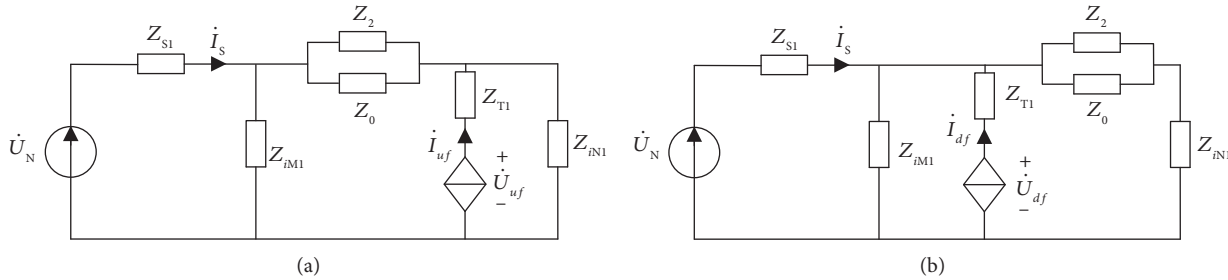

Figure 1: Composite sequence network of the break fault: (a) upstream of DG and (b) downstream of DG.

where Z_2 is the equivalent impedance of the negative sequence network and Z_0 is the equivalent impedance of the zero sequence network that can be computed as

$$Z_2 = \frac{Z_{S2}Z_{iM2}}{Z_{S2} + Z_{iM2}} + Z_{iN2}, \tag{8}$$

$$Z_0 = \frac{3Z_g}{1 + j3\omega Z_g C_{iM}} + \frac{1}{j\omega C_{iN}}, \tag{9}$$

where Z_{T1} is the DG step-up transformer impedance, Z_{S1} and Z_{S2} are the positive and negative sequence system equivalent impedances, Z_{iM1} and Z_{iM2} are the positive and negative sequence load impedances upstream of the fault point, Z_{iN1} and Z_{iN2} are the positive and negative sequence load impedances downstream of the fault point, Z_g is the neutral grounding impedance, C_{iM} is the capacitance upstream of the fault point, and C_{iN} is the capacitance downstream of the fault point.

From (7), $\dot{I}_{uf}$ can be expressed as

$$\dot{I}_{uf} = \frac{-\dot{U}_N + \sqrt{\dot{U}_N^2 + 8(2Z_{T1} + Z_{iN1})S_{\mathrm{DG}}}}{2(2Z_{T1} + Z_{iN1})}. \tag{10}$$

When a break fault occurs downstream of DG, according to (6), the composite sequence network can be established as shown in Figure 1(b). $\dot{I}_{df}$ and $\dot{U}_{df}$ denote the DG current and terminal voltages in case of a downstream break fault. The relationship between voltage and current is expressed as

$$\begin{cases} \dot{U}_N = \dot{I}_S Z_{S1} + (\dot{I}_S + \dot{I}_{df}) \cdot Z_{\Sigma 1}, \\ \dot{U}_{df} = \dot{I}_{df} Z_{T1} + (\dot{I}_S + \dot{I}_{df}) \cdot Z_{\Sigma 1}, \end{cases} \tag{11}$$

where $Z_{\Sigma 1}$ is the parallel equivalent impedance and can be expressed as

$$Z_{\Sigma 1} = Z_{iM1}(\|Z_2\|Z_0 + Z_{iN1}). \tag{12}$$

From (11), $\dot{I}_{df}$ can be expressed as

$$\dot{I}_{df} = \frac{-\dot{U}_N + \sqrt{\dot{U}_N^2 + 4((Z_{S1} + Z_{T1} + Z_{S1}Z_{T1})/Z_{\Sigma 1})S_{\mathrm{DG}}}}{2((Z_{S1} + Z_{T1} + Z_{S1}Z_{T1})/Z_{\Sigma 1})}. \tag{13}$$

Relative to normal operations, the DG current changes in the presence of a break fault. Combining (10) and (13) reveals that the DG break fault current is related to DG power, system impedance, system voltage, and load impedance. When the DG power S_{DG}, system impedance Z_S, and voltage $\dot{U}_N$ are determined, the DG break fault current is mainly affected by load impedance. The DG break fault current changes at different fault locations. According to (10) to (13), $\dot{I}_{uf}$ decreases as Z_{iN1} increases, whereas $\dot{I}_{df}$ increases along with Z_{iN1}. Meanwhile, Z_{iN1} decreases as the distance between the fault location and bus increases. The characteristics of the variation in DG break fault current along with fault location are shown in Figure 2. When the break fault occurs upstream of DG, a closer distance between the fault location and the head of the feeder corresponds to a smaller Z_{iN1} and a greater DG break fault current. Meanwhile, a closer distance between the fault location and the DG grid-connected point corresponds to a larger Z_{iN1} and a smaller DG break fault current. When the break fault occurs downstream of DG, a closer distance between the fault location and the DG grid-connected point corresponds to a smaller $Z_{\Sigma 1}$ and DG break fault current. Similarly, a closer distance between the fault location and the end of the feeder corresponds to a larger $Z_{\Sigma 1}$ and DG break fault current.

4. Break Fault Identification Method

According to (1), DG can be equivalent to a voltage-controlled current source in normal operations. In this case, the relationship between voltage and current can be expressed as

$$\begin{cases} \dot{U}_N = \dot{I}_S Z_{S1} + (\dot{I}_S + \dot{I}_n) \cdot (Z_{iM1}Z_{iN1}), \\ \dot{U}_n = \dot{I}_n Z_{T1} + (\dot{I}_S + \dot{I}_n) \cdot (Z_{iM1}Z_{iN1}), \end{cases} \tag{14}$$

where $\dot{I}_n$ and $\dot{U}_n$ are the DG current and terminal voltages in the normal operation, respectively.

From (14), $\dot{I}_n$ can be expressed as

$$\dot{I}_n = \frac{-\dot{U}_N + \sqrt{\dot{U}_N^2 + 4[(Z_{S1} + Z_{T1} + Z_{S1}Z_{T1})/Z_{iL1}]S_{\mathrm{DG}}}}{2[(Z_{S1} + Z_{T1} + Z_{S1}Z_{T1})/Z_{iL1}]}, \tag{15}$$

$$Z_{iL1} = \frac{Z_{iM1}Z_{iN1}}{Z_{iM1} + Z_{iN1}}, \tag{16}$$

where Z_{iL1} is the total positive sequence load impedance.

Combining (10), (13), and (15) reveals that when a break fault occurs upstream of DG, the variation in DG current relative to that under normal operations is formulated as

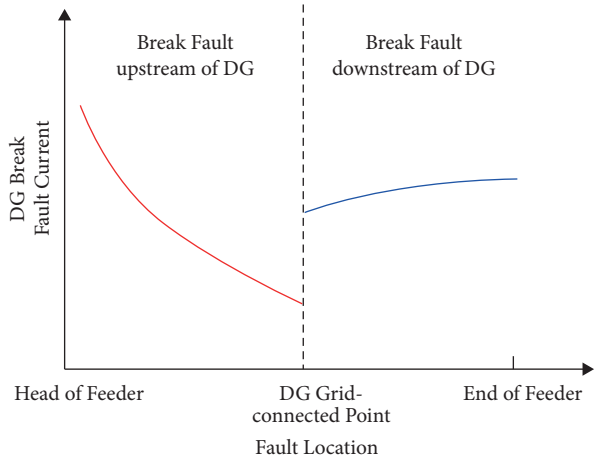

Figure 2: Characteristics of DG break fault current.

$$\Delta\dot{I}_{uf} = \frac{-\dot{U}_N + \sqrt{\dot{U}_N^2 + 8Z_{uf}S_{\mathrm{DG}}}}{2Z_{uf}} - \frac{-\dot{U}_N + \sqrt{\dot{U}_N^2 + 4Z_nS_{\mathrm{DG}}}}{2Z_n}. \tag{17}$$

When a break fault occurs downstream of DG, the variation in DG current relative to that under normal operations is formulated as

$$\Delta\dot{I}_{df} = \frac{-\dot{U}_N + \sqrt{\dot{U}_N^2 + 4Z_{df}S_{\mathrm{DG}}}}{2Z_{df}} - \frac{-\dot{U}_N + \sqrt{\dot{U}_N^2 + 4Z_nS_{\mathrm{DG}}}}{2Z_n}, \tag{18}$$

where, $Z_n = ((Z_{S1} + Z_{T1} + Z_{S1}Z_{T1})/Z_{iL1})$, $Z_{uf} = 2Z_{T1} + Z_{iN1}$, and $Z_{df} = ((Z_{S1} + Z_{T1} + Z_{S1}Z_{T1})/Z_{\Sigma 1})$.

Combined with (17), when $\Delta\dot{I}_{uf} > 0$, the equation can be solved as

$$S_{\mathrm{DG}} < S_t = \frac{Z_{uf} - Z_n}{\left(Z_{uf} - 2Z_n\right)^2}\dot{U}_N^2, \tag{19}$$

where S_t is the zero-crossing power.

Combined with (20), when $(\mathrm{d}\Delta\dot{I}_{uf}/\mathrm{d}S_{\mathrm{DG}}) = 0$, the equation can be solved as

$$S_r = \frac{3\dot{U}_N^2}{8\left(Z_{uf} - 2Z_n\right)}, \tag{20}$$

where S_r is the power at the extreme point.

When a break fault occurs upstream of DG, the DG current may be higher or lower than that under normal operations. Equation (17) shows that the DG current variation is mainly determined by DG power and load impedance. The DG current increases when $S_{\mathrm{DG}} < S_t$ but decreases when $S_{\mathrm{DG}} > S_t$. Given that Z_{S1} and Z_{T1} are much smaller than Z_{iN1}, $S_r < S_t$ always holds, that is, the power at the extreme point is less than that at the zero-crossing point. The curve of the DG current variation $\Delta\dot{I}_{uf}$ when a break fault occurs upstream of DG is shown in Figure 3. When $S_{\mathrm{DG}} < S_r$, $\Delta\dot{I}_{uf}$ increases along with power.

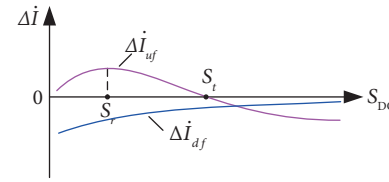

Figure 3: Change of DG current variation with S_{DG}.

When $S_{\mathrm{DG}} > S_r$, $\Delta\dot{I}_{uf}$ decreases along with increasing power and crosses zero at $S_{\mathrm{DG}} = S_t$.

Combined with (18), when $\Delta\dot{I}_{df} < 0$, this equation can be solved as

$$\left(Z_n - Z_{df}\right)^2 > 0. \tag{21}$$

Let $(\mathrm{d}\Delta\dot{I}_{df}/\mathrm{d}S_{\mathrm{DG}}) > 0$, which can be solved as

$$Z_n > Z_{df}. \tag{22}$$

The load impedance of distribution networks is often significantly greater than the system impedance, and the capacitive reactance of feeders is significantly greater than the load impedance. Therefore, equations (12) and (16) can be expressed as

$$Z_{\Sigma 1} \approx \frac{Z_{iM1}\left(Z_{iN1} + Z_{iN2}\right)}{Z_{iM1} + Z_{iN1} + Z_{iN2}}, \qquad Z_{iL1} = \frac{Z_{iM1}Z_{iN1}}{Z_{iM1} + Z_{iN1}}. \tag{23}$$

If $Z_{iN2} = kZ_{iN1}$, the ratio of Z_{iL1} to $Z_{\Sigma 1}$ can be expressed as

$$\frac{Z_{iL1}}{Z_{\Sigma 1}} = \frac{\left(Z_{iN1} + Z_{iM1}\right)/(1+k)}{Z_{iN1} + Z_{iM1}}. \tag{24}$$

When a break fault occurs downstream of DG, equation (24) shows that a larger k corresponds to a smaller deviation between Z_{iL1} and $Z_{\Sigma 1}$, whereas a smaller deviation between Z_n and Z_{df} corresponds to a smaller variation in the DG current. Combined with (18), given that $Z_{iL1} < Z_{\Sigma 1}$, $Z_n > Z_{df}$ can be obtained. In other words, equations (21) and (22) are always true. Therefore, the DG current variation $\Delta\dot{I}_{df}$ always increases along with S_{DG} when a break fault occurs downstream of DG as shown in Figure 3. $\dot{I}_{df}$ is always smaller than $\dot{I}_n$.

When the DG output current increases or decreases beyond the setting value, a break fault occurs upstream of DG. The setting value is determined by the maximum DG current variation in the case of a break fault downstream of DG. Therefore, the fault identification criterion can be expressed as

$$\Delta I_{\mathrm{DG}} < I_{ZD}, \quad \text{or } \Delta I_{\mathrm{DG}} > 0, \tag{25}$$

where ΔI_{DG} is the DG current variation and $I_{Z\,D}$ is the setting value of DG current variation that can be calculated as

$$\Delta I_{\mathrm{DG}} = I_{\mathrm{DG}}^{t} - I_{\mathrm{DG}}^{t-1}, \tag{26}$$

$$I_{ZD} = K_{\mathrm{rel}}\left(I_{df\cdot\min} - I_n\right) - I_E, \tag{27}$$

$$I_{df\cdot\min} = \left|\frac{-\dot{U}_N + \sqrt{\dot{U}_N^2 + 4Z_{df\cdot\max}S_{\mathrm{DG}}}}{2Z_{df\cdot\max}}\right|, \tag{28}$$

$$Z_{df\cdot\max} = \frac{Z_{S1} + Z_{T1} + Z_{S1}Z_{T1}}{Z_{\Sigma 1\cdot\min}}, \tag{29}$$

$$Z_{\Sigma 1\cdot\min} = \frac{(1+k)Z_{iL1}}{(1+k-kZ_{iL1})/Z_{iN1\cdot\max}}, \tag{30}$$

where I_{DG}^{t} is the DG output current at time t, I_{DG}^{t-1} is the DG output current at time t-1, K_{rel} is the reliability factor that ranges between 1.1 and 1.2, I_E is the error margin, $I_{df\cdot\min}$ is the minimum DG current in the case of a break fault downstream of DG, I_n is the DG output current under normal operations, $Z_{df\cdot\max}$ is the maximum value of Z_{df}, $Z_{\Sigma 1\cdot\min}$ is the minimum value of $Z_{\Sigma 1}$, $Z_{i\mathrm{N}1\cdot\max}$ is the maximum value of Z_{iN1} that is equal to the positive sequence load impedance at the end of the feeder, and k is the ratio of negative sequence impedance to positive sequence impedance of load.

When $Z_{S1} \ll Z_{iL1}$ and $Z_{S1} \ll Z_{\Sigma 1\cdot\max}$, one may obtain $Z_n \approx Z_{df\cdot\min}$. In other words, the DG output current remains unchanged under the presence of a break fault downstream of DG. Given the influence of actual measurement errors and to ensure the sensitivity of the break fault identification criterion, the error margin I_E in (27) can be set between 2 A and 5 A.

5. Break Fault Location Algorithm for Active Distribution Networks

The presence of multiple DGs on the feeder is equivalent to having multiple controlled sources connected in parallel upstream or downstream of the fault point. Given that the structure of the composite sequence network is unchanged, the characteristics of the DG break fault current and the break fault identification criteria remain valid. As shown in Figure 4, each DG grid-connected point is defined as a node and is represented by ①, ②, ③, ④, and ⑤. Meanwhile, the section between the node and bus or between two nodes is defined as the area and is denoted by (1), (2), (3), (4), and (5). Therefore, the network topology matrix **D** can be constructed as

$$D = \begin{bmatrix} 1 & 0 & 0 & 0 & 0 \\ -1 & 1 & 0 & 0 & 0 \\ 0 & -1 & 1 & 0 & 0 \\ 0 & 0 & 0 & 1 & 0 \\ 0 & 0 & 0 & -1 & 1 \end{bmatrix}. \tag{31}$$

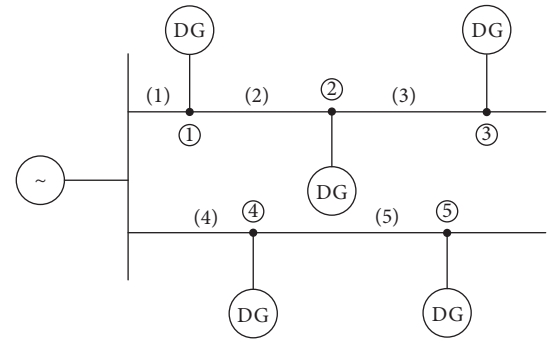

Figure 4: Schematic diagram of ADN.

The elements of the network topology matrix **D** are defined as

$$d_{ij} = \begin{cases} 1, & \text{area } i \text{ is upstream of node } j, \\ -1, & \text{area } i \text{ is downstream of node } j, \\ 0, & \text{other.} \end{cases} \tag{32}$$

The elements of the fault information matrix **F** are defined as

$$f_{ii} = \begin{cases} 1, & \text{DG of node } i \text{ satisfies fault identification criterion,} \\ 0, & \text{other.} \end{cases} \tag{33}$$

The fault location matrix **P** is defined as

$$P = D \cdot F. \tag{34}$$

Matrix **D** represents the positional relationship between areas and nodes, whereas matrix **F** represents the information of nodes downstream of the break fault. Therefore, matrix **P** can reflect the upstream, downstream, and fault point areas of a break fault. Each row element of matrix **P** presents the fault information of the corresponding area. If all elements in the row of matrix **P** are 0, then this row presents information on the upstream area of the break fault. If the row elements contain −1 and 1 and if the sum of elements is 0, then this row presents information on the downstream area of the break fault. If the row elements only contain 0 and 1 and if the sum of these elements is 1, then this row presents information on the break fault area.

As shown in Figure 4, if a break fault occurs in area (2), then the fault information matrix **F** can be built as

$$F = \begin{bmatrix} 0 & 0 & 0 & 0 & 0 \\ 0 & 1 & 0 & 0 & 0 \\ 0 & 0 & 1 & 0 & 0 \\ 0 & 0 & 0 & 0 & 0 \\ 0 & 0 & 0 & 0 & 0 \end{bmatrix}. \tag{35}$$

The fault location matrix **P** can be calculated as

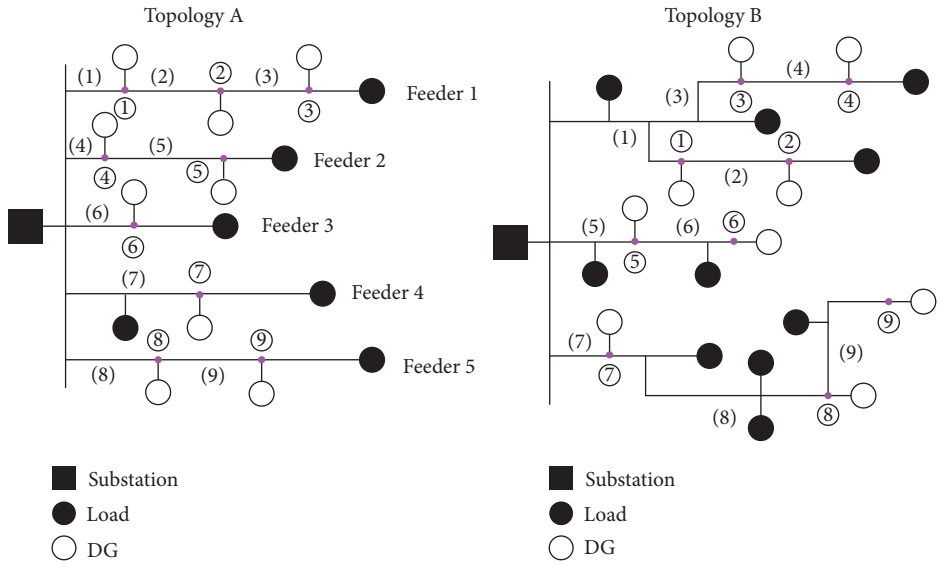

Figure 5: Schematic diagram of different topologies.

$$P = \begin{bmatrix} 0 & 0 & 0 & 0 & 0 \\ 0 & 1 & 0 & 0 & 0 \\ 0 & -1 & 1 & 0 & 0 \\ 0 & 0 & 0 & 0 & 0 \\ 0 & 0 & 0 & 0 & 0 \end{bmatrix}. \tag{36}$$

Equation (36) shows that areas (1), (4), and (5) are the upstream areas of the break fault, area (3) is the downstream area of the break fault, and area (2) is the break fault area.

The flow of the ADN break fault location algorithm is described as follows: First, the DGs are numbered, and the network topology matrix **D** is formed. Second, the output current of each DG is monitored at each time. Third, the setting value and actual variation in the DG current are calculated to check whether the break fault identification criterion is satisfied. Fourth, the DG information of each node is integrated to form the fault information matrix **F**. Finally, the fault location matrix **P** is calculated, and the break fault area is determined according to the characteristics of each row of matrix **P**.

6. Cases

To verify the reliability of the proposed method, a 10 kV ADN model was built in Matlab/Simulink as shown in Topology A in Figure 5. The distribution network has 5 feeders, and the positive sequence parameters are $r_1 = 0.031\Omega$/km, $l_1 = 0.096$ mH/km, and $c_1 = 0.338\,\mu$F/km. Meanwhile, the zero sequence parameters are $r_0 = 0.234\Omega$/km, $l_0 = 0.355$ mH/km, and $c_0 = 0.265\,\mu$F/km. The neutral point is grounded with a small resistance R_d of 10 Ω. The system equivalent impedance is 0.5 Ω, and the DG step-up transformer impedance is 1 Ω. The loads are kept static, and the parameters of loads and DGs are shown in Table 1.

All DGs and areas in the system are numbered according to the sequence of feeders and the distance between the node and bus. The nodes on feeder 1 are labeled ①, ②, and ③, which constitute areas (1), (2), and (3), respectively. The nodes on feeder 2 are labeled ④ and ⑤, which constitute areas (4) and (5), respectively. The nodes on feeders 3 and 4 are labeled ⑥ and ⑦, respectively, which constitute areas (6) and (7). The nodes on feeder 5 are labeled ⑧ and ⑨, which constitute areas (8) and (9), respectively.

Following the definition of (30), the network topology matrix **D** is constructed as

$$D = \begin{bmatrix} 1 & 0 & 0 & 0 & 0 & 0 & 0 & 0 & 0 \\ -1 & 1 & 0 & 0 & 0 & 0 & 0 & 0 & 0 \\ 0 & -1 & 1 & 0 & 0 & 0 & 0 & 0 & 0 \\ 0 & 0 & 0 & 1 & 0 & 0 & 0 & 0 & 0 \\ 0 & 0 & 0 & -1 & 1 & 0 & 0 & 0 & 0 \\ 0 & 0 & 0 & 0 & 0 & 1 & 0 & 0 & 0 \\ 0 & 0 & 0 & 0 & 0 & 0 & 1 & 0 & 0 \\ 0 & 0 & 0 & 0 & 0 & 0 & 0 & 1 & 0 \\ 0 & 0 & 0 & 0 & 0 & 0 & 0 & -1 & 1 \end{bmatrix}. \tag{37}$$

By combining 27–31 with the parameters shown in Table 1, the setting values of the DG current variation in each node are calculated as shown in Table 2, where K_{rel} is 1.1 and I_E is 2 A.

When $t = 0.3$ s, a single-phase break fault occurs at 3 km of feeder 1. The variation in the DG output current before and after the fault is presented in Figure 6, which shows that the amplitude of the DG output current at nodes ② and ③ significantly increases, whereas the other nodes remain unchanged after the occurrence of the break fault. The DG output current of each node is recorded in Table 3. The DG current variation before and after the occurrence of a break fault at nodes ① and ④ to ⑨ ranges from approximately 0.1 A to 0.2 A. The DG

Table 1: Parameters of loads and DGs.

Feeder number	Length (km)	Load (MW)	Location (km)	S_{DG} (MW)	Location (km)
1	10	5	10	1, 0.5, 0.3	2, 5, 8
2	7	6	7	1.5, 0.5	1, 5
3	5	10	5	2	3
4	8	2, 4	2, 8	1.6	4
5	9	8	9	3, 1	3, 6

Table 2: Setting value calculation.

Node	I_{ZD} (A)
1	−2.1
2	−2.1
3	−2.0
4	−2.2
5	−2.1
6	−3.3
7	−2.3
8	−3.5
9	−2.2

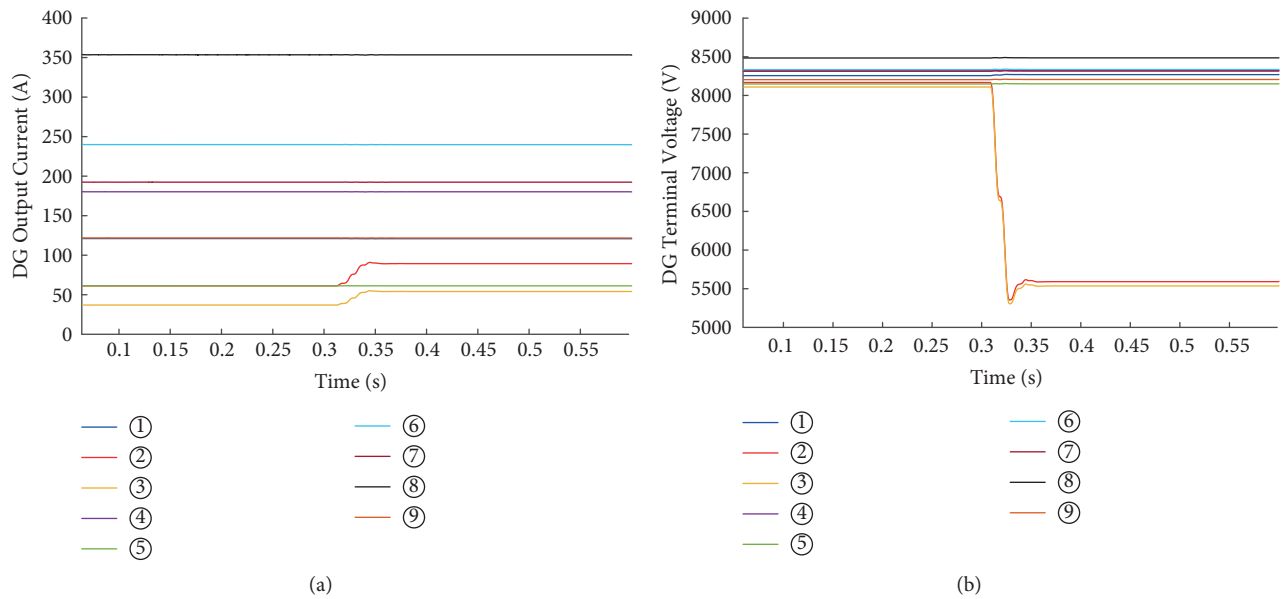

Figure 6: Variation of DG output current and terminal voltage. (a) DG output current. (b) DG terminal voltage.

Table 3: DG output current.

Node	DG output current (A)		DG current variation (A)
	Before break fault	After break fault	
1	121.1	120.9	−0.2
2	61.2	89.4	28.2
3	37	54.2	17.2
4	180.3	180.2	−0.1
5	61.4	61.3	−0.1
6	240.0	239.9	−0.1
7	192.5	192.4	−0.1
8	353.6	353.4	−0.2
9	121.9	121.8	−0.1

current variation at nodes ② and ③ is about tens of Amperes. A greater DG power corresponds to a greater variation. The DG current variation of each node is compared with the corresponding setting value according to Tables 2 and 3. Nodes ① and ④ to ⑨ satisfy $I_{ZD} < \Delta I_{DG} < 0$, whereas nodes ② and ③ satisfy $\Delta I_{DG} > 0 > I_{ZD}$. By combining (25) and (33), the fault information matrix **F** can be constructed as

$$F = \begin{bmatrix} 0&0&0&0&0&0&0&0&0 \\ 0&1&0&0&0&0&0&0&0 \\ 0&0&1&0&0&0&0&0&0 \\ 0&0&0&0&0&0&0&0&0 \\ 0&0&0&0&0&0&0&0&0 \\ 0&0&0&0&0&0&0&0&0 \\ 0&0&0&0&0&0&0&0&0 \\ 0&0&0&0&0&0&0&0&0 \\ 0&0&0&0&0&0&0&0&0 \end{bmatrix}. \quad (38)$$

According to (34), the fault location matrix **P** can be calculated as

$$P = \begin{bmatrix} 0&0&0&0&0&0&0&0&0 \\ 0&1&0&0&0&0&0&0&0 \\ 0&-1&1&0&0&0&0&0&0 \\ 0&0&0&0&0&0&0&0&0 \\ 0&0&0&0&0&0&0&0&0 \\ 0&0&0&0&0&0&0&0&0 \\ 0&0&0&0&0&0&0&0&0 \\ 0&0&0&0&0&0&0&0&0 \\ 0&0&0&0&0&0&0&0&0 \end{bmatrix}. \quad (39)$$

Given that the elements in rows 1 and 4 to 9 of matrix **P** are all 0, areas (1), (4), (5), (6), (7), (8), and (9) represent the upstream area of the break fault. The elements in row 3 contain −1 and 1, and the sum of these elements is 0. Therefore, area (3) is selected as the downstream area of the break fault. The elements in row 2 only contain 0 and 1, and the sum of these elements is 1. Therefore, area (2) is selected as the break fault area; that is, a break fault occurs in the section between nodes ② and ③.

The resulting DG current variation before and after the fault in different fault locations is shown in Table 4. As can be seen from the table, when the fault is located 1 or 2 km away from the bus, the DG current variation of nodes ④ to ⑨ is very small and negative, whereas that of nodes ①, ②, and ③ is positive and satisfies the break fault identification criterion. Area (1) can be selected as the break fault area based on the proposed matrix algorithm. Similarly, when the fault location is 3, 4, or 5 km away from the bus, area (2) can be selected as the break fault area. When the fault location is 6, 7, or 8 km away from the bus, area (3) can be selected as the break fault area. Therefore, the proposed method can reliably locate break faults at different locations and areas.

The S_t corresponding to each node is calculated using (19) and shown in Table 5. The S_{DG} of each node in Table 1 is less than the calculated S_t. The analysis in Section 3 reveals that regardless of the break fault location, the output current of the DG downstream of the fault point always increases. The simulation results in Table 3 are consistent with the results of the theoretical analysis.

To verify the effectiveness of the proposed method under different DG power values, only the S_{DG} of node ② is changed. The DG current variation is shown in Table 6. When the S_{DG} of node ② is less than the corresponding S_t (5.6 MW), the DG output current increases after the occurrence of a break fault. When the S_{DG} of node ② is greater than the corresponding S_t, the DG output current decreases. As the S_{DG} increases, the DG current variation initially increases and then decreases. These simulation results are consistent with those of the theoretical analysis. Obviously, under various DG power values, node ② always satisfies the break fault identification criterion. Therefore, the fault information matrix **F** and fault location matrix **P** do not change, the fault area is still area (2), and the fault location is deemed accurate.

In order to verify the scalability of the proposed method, the structure of the ADN model is changed to Topology B as shown in Figure 5. The matrix D' of Topology B is constructed as

$$D' = \begin{bmatrix} 1&0&0&0&0&0&0&0&0 \\ -1&1&0&0&0&0&0&0&0 \\ -1&0&1&0&0&0&0&0&0 \\ 0&0&-1&1&0&0&0&0&0 \\ 0&0&0&0&1&0&0&0&0 \\ 0&0&0&0&-1&1&0&0&0 \\ 0&0&0&0&0&0&1&0&0 \\ 0&0&0&0&0&0&-1&1&0 \\ 0&0&0&0&0&0&0&-1&1 \end{bmatrix}. \quad (40)$$

When a break fault occurs in area (3), the DG current variation of nodes ① to ⑨ are −0.1, −0.1, 7.7, 35.7, −0.1, −0.1, −0.2, and −0.1 A, respectively. Thus, the fault information matrix F' can be constructed as

$$F' = \begin{bmatrix} 0&0&0&0&0&0&0&0&0 \\ 0&0&0&0&0&0&0&0&0 \\ 0&0&1&0&0&0&0&0&0 \\ 0&0&0&1&0&0&0&0&0 \\ 0&0&0&0&0&0&0&0&0 \\ 0&0&0&0&0&0&0&0&0 \\ 0&0&0&0&0&0&0&0&0 \\ 0&0&0&0&0&0&0&0&0 \\ 0&0&0&0&0&0&0&0&0 \end{bmatrix}. \quad (41)$$

Then, the fault location matrix P' can be calculated as

Table 4: DG current variation in different fault locations.

Fault location (km)	DG current variation of each node (A)								
	1	2	3	4	5	6	7	8	9
1	24.3	12.5	7.6	−0.1	−0.1	−0.1	−0.1	−0.2	−0.1
2	24.3	12.5	7.6	−0.1	−0.1	−0.1	−0.1	−0.2	−0.1
3	−0.2	28.2	17.2	−0.1	−0.1	−0.1	−0.1	−0.2	−0.1
4	−0.1	28.2	17.2	−0.1	−0.1	−0.1	−0.1	−0.2	−0.1
5	−0.1	28.2	17.2	−0.1	−0.1	−0.1	−0.1	−0.2	−0.1
6	−0.1	−0.2	26.4	−0.1	−0.1	−0.1	−0.1	−0.2	−0.1
7	−0.1	−0.2	26.4	−0.1	−0.1	−0.1	−0.1	−0.2	−0.1
8	−0.1	−0.2	26.4	−0.1	−0.1	−0.1	−0.1	−0.2	−0.1

Table 5: S_t of each node.

Node	S_t (MW)
1	5.7
2	5.7
3	5.7
4	6.2
5	6.2
6	13.2
7	4.2
8	9.9
9	9.9

Table 6: DG output current under different S_{DG} of node ②.

S_{DG} (MW)	DG output current (A)		DG current variation (A)
	Before break fault	After break fault	
0.5	61.2	89.4	28.2
1	121.4	158.5	37.1
2	238.8	268.1	29.3
3	352.5	356.9	4.4
4	463.1	465.4	2.3
6	675.3	563.9	−111.4
7	777.4	621.5	−155.9

$$P' = \begin{bmatrix} 0 & 0 & 0 & 0 & 0 & 0 & 0 & 0 & 0 \\ 0 & 0 & 0 & 0 & 0 & 0 & 0 & 0 & 0 \\ 0 & 0 & 1 & 0 & 0 & 0 & 0 & 0 & 0 \\ 0 & 0 & -1 & 1 & 0 & 0 & 0 & 0 & 0 \\ 0 & 0 & 0 & 0 & 0 & 0 & 0 & 0 & 0 \\ 0 & 0 & 0 & 0 & 0 & 0 & 0 & 0 & 0 \\ 0 & 0 & 0 & 0 & 0 & 0 & 0 & 0 & 0 \\ 0 & 0 & 0 & 0 & 0 & 0 & 0 & 0 & 0 \\ 0 & 0 & 0 & 0 & 0 & 0 & 0 & 0 & 0 \end{bmatrix}. \quad (42)$$

At present, phase voltage rise and phase current sag are usually used to identify break faults in substations. In order to compare with the proposed method, load parameters of feeder 1 in Table 1 are reset. Loads of 1, 1.5, 2, and 0.5 MW are connected to 1, 4, 6, and 10 km of feeder 1, respectively. When a single-phase break fault occurs at 7 km of feeder 1, the phase current variation of feeder 1 is −3.8 A. The phase current is only reduced by 2%. The phase current decreases slightly, which is difficult to distinguish from normal operating conditions such as load switching. However, in the proposed method, the output current variation of each DG is −0.1, −0.1, 2.5, −0.1, −0.1, −0.2, and −0.1 A, which can accurately reflect that the fault is located between node ② and node ③. Compared with the existing method, the advantage of the proposed method is that it is not affected by load size and distribution and has high reliability.

7. Conclusions

This paper proposes a new locating method of break faults in ADNs based on DG monitoring. The paper studies the DG output current variation characteristics when break faults occur upstream or downstream of DG. Based on the matrices constructed by the network topology and DG fault information, a break fault location algorithm is proposed.

The simulation verifies that the method is not affected by the changes of DG power, network topology, load, and fault location. The method has a good application effect in the ADN with a high proportion of DG. In addition, the algorithm is simple to calculate, highly feasible, and does not rely on external monitoring devices.

Data Availability

Data sharing not applicable to this article as no datasets were generated or analyzed during the current study.

Conflicts of Interest

The authors declare that there are no conflicts of interest regarding the publication of this paper.

Acknowledgments

This work was supported by the National Natural Science Foundation of China under Grant U1866603.

References

[1] V. Telukunta, J. Pradhan, J. Pradhan, M. Singh, and S. G. Srivani, "Protection challenges under bulk penetration of renewable energy resources in power systems: a review," *CSEE Journal of Power and Energy Systems*, vol. 3, no. 4, pp. 365–379, 2017.

[2] D. Xu, Q. Wu, B. Zhou, C. Li, L. Bai, and S. Huang, "Distributed multi-energy operation of coupled electricity, heating, and natural gas networks," *IEEE Transactions on Sustainable Energy*, vol. 11, no. 4, pp. 2457–2469, 2020.

[3] S. Roostaee, M. S. Thomas, and S. Mehfuz, "Experimental studies on impedance based fault location for long transmission lines," *Protection and Control of Modern Power Systems*, vol. 2, no. 2, pp. 169–177, 2017.

[4] L. Xie, L. Luo, Y. Li, Y. Zhang, and Y. Cao, "A traveling wave-based fault location method employing VMD-TEO for distribution network," *IEEE Transactions on Power Delivery*, vol. 35, no. 4, pp. 1987–1998, 2020.

[5] Y. Ye, X. Ma, X. Lin et al., "Active fault locating method based on SOP for single phase grounding faults in the resonant grounding distribution network," *Proceedings of the CSEE*, vol. 40, no. 5, pp. 1453–1465, 2020.

[6] J.-H. Teng, W.-H. Huang, and S.-W. Luan, "Automatic and fast faulted line-section location method for distribution systems based on fault indicators," *IEEE Transactions on Power Systems*, vol. 29, no. 4, pp. 1653–1662, 2014.

[7] P. Farzan, M. Izadi, C. Gomes, M. Z. A. A. Kadir, M. H. Hesamian, and M. A. M. Radzi, "On the fault location algorithm for distribution networks in presence of DG," in *Proceedings of the 2014 IEEE Innovative Smart Grid Technologies—Asia (ISGT Asia)*, Kuala Lumpur, Malaysia, 2014.

[8] K. Pandakov and H. K. Høidalen, "Distance protection with fault impedance compensation for distribution network with DG," in *Proceedings of the 2017 IEEE PES Innovative Smart Grid Technologies Conference Europe (ISGT-Europe)*, Turin, Italy, 2017.

[9] R. F. Buzo, H. M. Barradas, and F. B. Leao, "A new method for fault location in distribution networks based on voltage sag measurements," *IEEE Transactions on Power Delivery*, vol. 36, no. 2, pp. 651–662, 2021.

[10] G. Manassero, S. G. Di Santo, and L. Souto, "Heuristic method for fault location in distribution feeders with the presence of distributed generation," *IEEE Transactions on Smart Grid*, vol. 8, no. 6, pp. 2849–2858, 2017.

[11] K. Jiang, H. Wang, M. Shahidehpour, and B. He, "Block-sparse Bayesian learning method for fault location in active distribution networks with limited synchronized measurements," *IEEE Transactions on Power Systems*, vol. 36, no. 4, pp. 3189–3203, 2021.

[12] Y. Xiao, J. Ouyang, X. Xiong, Y. Wang, and Y. Luo, "Fault protection method of single-phase break for distribution network considering the influence of neutral grounding modes," *Protection and Control of Modern Power Systems*, vol. 5, no. 10, 2020.

[13] K. Wang, X. Xiong, Y. Xiao, and J. Ouyang, "Single-phase break fault protection method for an active distribution network based on negative sequence current," *Power System Protection and Control*, vol. 36, no. 6, pp. 10–18, 2021.

[14] Y. Xue, M. Chen, L. Cao, G. Feng, and B. Xu, "Analysis of voltage characteristics of single-phase disconnection fault in ungrounded distribution system," *Proceedings of the CSEE*, vol. 41, no. 4, pp. 1322–1333, 2021.

[15] J. Liu, Z. Zhang, and Y. Wang, "Voltage information based broken-line fault location for distribution network," *Automation of Electric Power Systems*, vol. 44, no. 21, pp. 123–131, 2020.

[16] L. Zhu, C. Li, H. Zhang, and Z. Zhang, "Negative sequence current distributing and single-phase open-line fault protection in distribution network," *Power System Protection and Control*, vol. 37, no. 9, pp. 35–38, 2009.

[17] Q. Kang, W. Cong, Y. Sheng, and Y. Wang, "Protection methods of single-phase broken-line fault for distribution line," *Power System Protection and Control*, vol. 47, no. 8, pp. 127–136, 2019.

[18] Z. Chang, G. Song, and W. Zhang, "Analysis on negative sequence voltage and current characteristics of single phase line breakage fault in distribution network and fault segment location," *Power System Technology*, vol. 44, no. 8, pp. 3065–3074, 2020.

[19] Z. Chang, G. Song, and X. Wang, "Identification and isolation of line breakage fault in distribution network based on zero sequence voltage amplitude differential principle," *Automation of Electric Power Systems*, vol. 42, no. 6, pp. 135–139, 2018.

[20] S. Wu, Y. Zhang, and Y. Su, "Open-line fault diagnosis based on data association of MV distribution network," *Electric Power Automation Equipment*, vol. 37, no. 7, pp. 101–109, 2017.

[21] S. Jamali, A. Bahmanyar, and S. Ranjbar, "Hybrid classifier for fault location in active distribution networks," *Protection and Control of Modern Power Systems*, vol. 5, no. 2, pp. 84–92, 2020.

[22] X. Fan, S. Sun, D. Sun, S. Hai, and Y. Wang, "Analysis of three-phase short-circuit current characteristics of doubly fed induction generator," *Power System Protection and Control*, vol. 47, no. 18, pp. 38–48, 2019.

[23] C. Wei, X. Shi, H. Zhang, S. Ci, and Y. Liu, "Fault model of IIDG with PQ control considering tracking capability of current command," *Electric Power Automation Equipment*, vol. 40, no. 1, pp. 59–65, 2020.

[24] W. Guo and L. Mu, "Fault model of inverter-based distributed generator considering flexible control strategy and current limitation," *Proceedings of the CSEE*, vol. 35, no. 24, pp. 6359–6367, 2015.

[25] X. Du, J. Ouyang, X. Long et al., "A protection method of a single-phase break fault for an active distribution network based on current change rates of distributed generation," *Power System Protection and Control*, vol. 48, no. 22, pp. 41–48, 2020.

[26] J. Ouyang, T. Tang, J. Yao, and M. Li, "Active voltage control for DFIG-based wind farm integrated power system by coordinating active and reactive powers under wind speed variations," *IEEE Transactions on Energy Conversion*, vol. 34, no. 3, pp. 1504–1511, 2019.

[27] M. Yousaf, K. M. Muttaqi, and D. Sutanto, "A control strategy to mitigate the sensitivity deterioration of overcurrent protection in distribution networks with the higher concentration of the synchronous and inverter-based DG units," *IEEE Transactions on Industry Applications*, vol. 57, no. 3, pp. 2298–2306, 2021.